A Letters Journal Exploring the Frontiers of Physics

December 2007

EPL, **80** (2007) 58001
doi: 10.1209/0295-5075/80/58001

www.epljournal.org

Force networks and the dynamic approach to jamming in sheared granular media

G. Lois[1,2] and J. M. Carlson[1]

[1] *Department of Physics, University of California - Santa Barbara, CA 93106-9530, USA*
[2] *Department of Physics, Department of Mechanical Engineering, Yale University - New Haven, CT 06520-8284, USA*

received 25 June 2007; accepted in final form 2 October 2007
published online 23 October 2007

PACS 81.05.Rm – Porous materials; granular materials
PACS 83.80.Fg – Granular solids
PACS 47.50.-d – Non-Newtonian fluid flows

Abstract – Diverging correlation lengths on either side of the jamming transition are used to formulate a rheological model of granular shear flow, based on the propagation of stress through force chain networks. The model predicts three distinct flow regimes, characterized by the shear rate dependence of the stress tensor, that have been observed in both simulations and experiments. The boundaries separating the flow regimes are quantitatively determined and testable. In the limit of jammed granular solids, the model predicts the observed anomalous scaling of the shear modulus and a new relation for the shear strain at yield.

Copyright © EPLA, 2007

Jamming occurs when an amorphous collection of particles spontaneously develops rigidity and supports weight like a solid instead of flowing like a liquid [1]. The transition takes place without static spatial ordering, but is accompanied by long-range dynamical correlations arising from the collective motion of groups of particles [2–4]. In the case of sheared granular materials, the transition from jammed to flowing phases occurs as the applied stress $\mathbf{\Sigma}$ is increased or the packing fraction ϕ is decreased, and there is a packing fraction ϕ_c at which the system jams in the limit of zero stress [5–7]. Diverging correlation lengths are observed on each side of the transition, and are related to the average size of force chain networks for $\phi < \phi_c$ [2,8] and the average size of isostatic clusters for $\phi > \phi_c$ [3,9].

In the jammed state many macroscopic observables exhibit power law scalings in $(\phi - \phi_c)$ [5–7] and the flowing state rheology changes dramatically as the packing fraction is increased above ϕ_c. Although the jamming transition controls both dynamic and static properties near ϕ_c, theories tend to focus mainly on the latter [9,10]. Here we theoretically explore the jamming transition by first considering flows with non-zero shear rate $\dot{\gamma}$ and then taking the limit of $\dot{\gamma} \to 0$ to access the static case. This procedure leads to quantitative predictions for the flowing rheology that match observations in ref. [11]. It also predicts the anomalous static scaling of the shear modulus measured in refs. [5,6] and a new scaling relation for the static yield strain, $\gamma^* \propto (\phi - \phi_c)^{1/2}$, which provides a testable prediction of the theory.

Granular materials behave as peculiar liquids. This can be clearly demonstrated by measuring the shear rate dependence of the stress tensor $\mathbf{\Sigma}(\dot{\gamma})$. Depending on various parameters, the system exhibits either Bagnold scaling $\mathbf{\Sigma} \propto \dot{\gamma}^2$, elastic-inertial scaling $\mathbf{\Sigma} \propto \dot{\gamma}^1$, or quasi-static scaling $\mathbf{\Sigma} \propto \dot{\gamma}^0$ (*i.e.* constant) [11]. The rheology of the flow is dependent on ϕ, with Bagnold scaling for $\phi < \phi_c$, quasi-static scaling for $\phi > \phi_c$, and elastic-inertial scaling in between. This is in marked contrast to Newtonian fluids where $\mathbf{\Sigma} \propto \dot{\gamma}$ and only the proportionality constant depends on ϕ. Although the phase diagram of granular shear flow has been extensively studied in simulations [11–13] and experiments [14], the origins of the rheological crossovers remain to be explained. Arriving at a solution to this problem requires a well-developed theory for the stress tensor in dense granular flows.

The stress tensor ultimately depends on the amorphous microscopic arrangement of grains. Forces are transmitted via contacts between grains and a perturbation on one grain can have long-range effects. Indeed, both experiments and simulations indicate that contact forces are correlated [2,15] and tend to form quasi–one-dimensional filaments, or force chains, that permeate the material [16]. Since contact between grains is the only form of force transfer, $\mathbf{\Sigma}$ is fully determined by properties of the networks [17,18]. Here we investigate the role of force chain

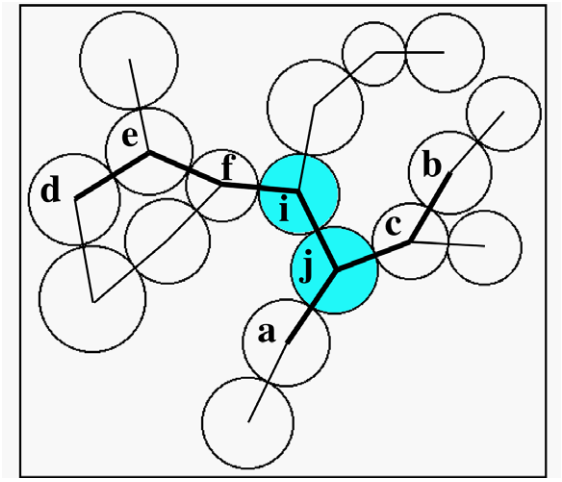

Fig. 1: A force network of grains taken from simulations [18]. The grains not connected to this particular cluster are not shown. In the FNM, the elastic force between grains i and j arises from collisional forces that propagate through the network. Lines are drawn between contacting grains, with the bold lines illustrating different paths through the network. The path $d \to e \to f \to i$ is defined as a path of length $\ell = 3$ since the collisional force $F_{\rm bc}^{de}$ must travel through three grains to affect the contact $\{i, j\}$. Also illustrated are paths of length $\ell = 1$ ($a \to j$) and $\ell = 2$ ($b \to c \to j$). At each link in a path, the transferred force is reduced by a factor $\mathcal{G}^{i'j'}(1)$, which depends on the relative angle between the contact and the amount of friction. The total elastic force is determined by summing over all possible paths through the network.

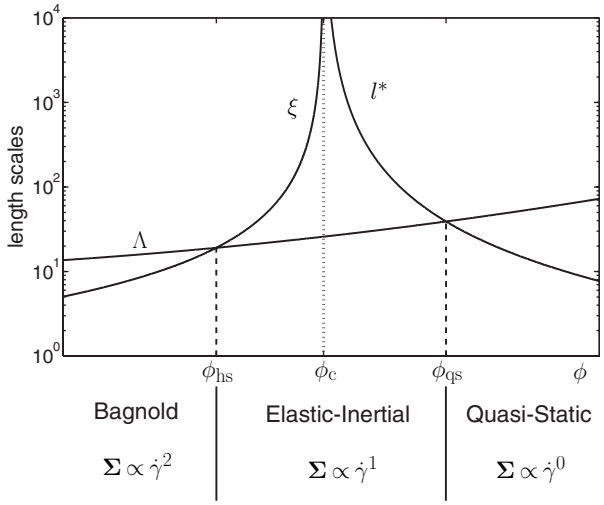

Fig. 2: A schematic illustration of three important length scales, plotted as a function of packing fraction ϕ, and their relation to granular flow near $\phi_{\rm c}$. ξ gives the average physical size of force chain networks and diverges as $\phi \to \phi_{\rm c}^-$. l^* quantifies the length scale above which the system responds as an elastic solid and diverges as $\phi \to \phi_{\rm c}^+$. $\Lambda \equiv c/\dot{\gamma}$ gives the maximum distance that forces, which propagate at an effective speed c, can become correlated. The macroscopic rheology (indicated beneath the graph) depends on the smallest length scale, and transitions occur at the intersections. $\phi_{\rm c}$ is the packing fraction where the system jams in the limit of zero stress. Our predictions for $\phi_{\rm hs}$ and $\phi_{\rm qs}$ are given in eqs. (4), (5).

networks in determining the value of the stress tensor by constructing a model of momentum transfer. We begin with an overview of the force network model (FNM) for perfectly rigid grains and then extend the model to include realistic grains with finite rigidity.

The force network model (FNM) for rigid grains. – The central concept of the FNM [18] is that the force F^{ij} between a pair of contacting grains $\{i, j\}$ can be expressed as the sum of a collisional part $F_{\rm bc}^{ij}$ and an elastic part $F_{\rm s}^{ij}$. The collisional part is the force expected from collisions between pairs of grains in the absence of networks. It is proportional to the square of the relative velocity between the contacting grains i and j upon initial incidence and is predicted by kinetic theory to scale with the square of the shear rate $\dot{\gamma}^2$ [19]. The elastic force is a consequence of the pressure induced by the network surrounding a pair of grains. Collisional forces from other contacts in the network are transferred to the pair from first nearest neighbors, second nearest neighbors, and so forth, all the way to the edge of the network, as illustrated in fig. 1. The presence of multiple contacts leads to an elastic force $F_{\rm s}^{ij}$ between grains i and j, and this contribution can be expressed as a sum over all paths between the contact $\{i, j\}$ and every other contact $\{i', j'\}$ in the connected force network:

$$F_{\rm s}^{ij} = \sum_{\ell=1}^{\xi-1} \sum_{\{i',j'\}} \mathcal{G}^{i'j'}(\ell) F_{\rm bc}^{i'j'}. \qquad (1)$$

In this equation, ℓ is the path length (in grain diameters) between two contacts $\{i, j\}$ and $\{i', j'\}$. The maximum path length is constrained by the average linear size of physical networks ξ, which has been measured in simulations by considering correlations between grain forces [2,18] and diverges as $\phi \to \phi_{\rm c}$, as plotted in fig. 2. $F_{\rm bc}^{i'j'}$ is the collisional force on the contact at the end of the path and the sum over $\{i', j'\}$ includes all collisional forces in the network, which may have multiple paths leading to the contact $\{i, j\}$. The function $\mathcal{G}^{i'j'}(\ell)$ accounts for the fact that only a fraction of the collisional force is transferred at each link in the path, and no more than the collisional force can be transferred from each contact in the network. In constructing this equation we assume that grains are perfectly rigid, which ensures that the propagation of collisional forces is instantaneous.

By defining $N(\ell)$ as the total number of contacts separated by path length ℓ, $\mathcal{G}(\ell)$ as the average of $\mathcal{G}^{i'j'}(\ell)$ over all paths of length ℓ, and $F_{\rm bc}$ as the average collisional force, eq. (1) reads

$$F_{\rm s}^{ij} = \sum_{\ell=1}^{\xi-1} N(\ell)\mathcal{G}(\ell)F_{\rm bc}(\ell). \qquad (2)$$

This is the central equation of the FNM: its parameters are related to the network geometry and have all been measured in simulations [18].

The FNM is similar to other models that separate the stress tensor into elastic and collisional components [20], but introduces a new way to calculate elastic stresses. Elastic stresses arise from clusters (not necessarily percolating) of simultaneously contacting grains that transfer forces. These force networks are not static, but are constantly formed and destroyed by the shear flow. Since each of these rates is proportional to $\dot{\gamma}$, properties of the steady-state networks are independent of $\dot{\gamma}$.

Bagnold scaling. – Equation (2) yields a constitutive relation for each component of the stress tensor that matches measurements from simulations for rigid grains with $\phi < \phi_c$ [18]. A major feature of the constitutive relations is that Bagnold scaling holds, *i.e.* $\mathbf{\Sigma} \propto \dot{\gamma}^2$. This is because all of the network parameters in eq. (2) are independent of $\dot{\gamma}$ and the rheology is set by F_{bc}, as predicted by kinetic theory [19].

The form of the constitutive relations is especially simple for rigid granular materials slightly below ϕ_c. At these large packing fractions, each grain has many contacts and the entire collisional force from every contact is transferred to its nearest neighbors. Thus $N(1)\mathcal{G}(1) = 1$, which implies that $N(\ell)\mathcal{G}(\ell) = 1$ for all ℓ. In this limit, it follows from eq. (2) that $\mathbf{\Sigma} \propto \xi F_{bc} \propto \xi\dot{\gamma}^2$. The FNM predicts that the stress tensor is proportional to the size of the force networks, independent of spatial dimension. For dense flows with $\xi \gg 1$ it also predicts that the collisional part of the stress, proportional to F_{bc}, is much smaller than the elastic part, proportional to $(\xi - 1)F_{bc}$, which has been observed in simulations [18].

The elastic-inertial regime. – The FNM has been constructed for perfectly rigid grains by assuming that forces propagate instantaneously through networks. Now we extend the model to realistic grains with finite stiffness, where forces propagate at finite speed. Because forces do not propagate instantaneously, even if physical networks exist with size ξ, forces might not reach the end of a network before it is destroyed. Therefore, in addition to ξ, it is important to consider the maximum extent of *correlated* networks Λ for grains with finite stiffness.

The value of Λ is difficult to predict. It is proportional to the elastic speed that forces move through individual grains (dependent on grain stiffness) and inversely proportional to the rate $\dot{\gamma}$ at which networks are destroyed [11,12]. However, it is more complicated than this and depends sensitively on network topology, since oftentimes breaking even a single contact can sever a network and prevent forces from propagating. We will therefore set $\Lambda \equiv c/\dot{\gamma}$, which defines c as the effective speed that forces propagate through networks. While c increases with grain stiffness it also depends on the topology of the networks and will thereby increase with packing fraction, since denser packed networks have a larger number of paths between any two grains. For flows of grains with finite stiffness and $\dot{\gamma} > 0$, Λ is always finite and is plotted in fig. 2.

For realistic grains there are two relevant length scales for $\phi < \phi_c$: the size of the physical contact networks ξ and the maximum correlation distance Λ. If $\xi < \Lambda$ then forces propagate through the entire physical network before it is destroyed. Therefore the assumptions of the rigid grain FNM hold and $\mathbf{\Sigma} \propto \xi\dot{\gamma}^2$, averaged over time scales larger than ξ/c. However, if $\xi > \Lambda$, the collisional force from a single contact is not transferred to the entire network, but only over a distance Λ. Since ξ diverges at ϕ_c, there is always a critical packing fraction ϕ_{hs} above which $\Lambda < \xi$, as illustrated in fig. 2. For $\phi > \phi_{hs}$ the shear flow is in a regime where the size of the physical networks ξ becomes irrelevant and must be replaced by the size of correlated networks Λ. This predicts a linear scaling of stress with shear rate, $\mathbf{\Sigma} \propto c\dot{\gamma}$, as was observed in ref. [11] and named the elastic-inertial regime.

The introduction of finite grain stiffness to the FNM produces a crossover from Bagnold's scaling to elastic-inertial scaling as the packing fraction is increased. The elastic-inertial scaling reveals that a second time scale, shown here to be dependent on the speed of force propagation through force networks, becomes important at high packing fraction.

The onset of quasi-static flow. – For $\phi > \phi_c$, a third length scale l^* becomes relevant [9] that is related to the departure from the isostatic limit. Isostatically jammed materials are configured such that contact forces can be completely determined from the constraint that no particle moves [21]. This occurs when the coordination number z, equal to the average number of contacts per particle, approaches a critical value z_c that depends on the spatial dimension. Contact forces are highly correlated in the isostatic state since breaking any single contact alters the value of every other contact force and causes rearrangements of grains over the entire material.

For a system with $z = z_c + \delta z$ $(\delta z > 0)$, large-scale rearrangements are confined to small distances and elasticity is recovered over length scales larger than l^*. It was predicted that $l^* \propto 1/\delta z$ [9] and this scaling has been verified in simulations [3]. Although these simulations were constrained by system size to $l^* \leqslant 20$ grain diameters, the scaling is expected [9] to hold as $l^* \to \infty$. The value of l^* is related to the packing fraction, since $\delta z \propto (\phi - \phi_c)^{1/2}$ [5,6], and is plotted in fig. 2.

The rheology of granular shear flow with $\phi > \phi_c$ depends on the relative sizes of the correlated networks Λ and isostatic clusters l^*. When $l^* > \Lambda$ forces propagate over regions where grain rearrangements are prevalent and inertial scalings are therefore important. When $l^* < \Lambda$ forces propagate over distances that are large compared to the rearranging regions, redundant contacts stabilize the networks, and forces are no longer inertial. At $l^* = \Lambda \equiv c/\dot{\gamma}$ the rheology crosses over from elastic-inertial behavior,

$\mathbf{\Sigma} \propto c\dot{\gamma}$ for $\Lambda \leqslant l^*$, to quasi-static scaling, $\mathbf{\Sigma} \propto c^2/l^*$ for $\Lambda \geqslant l^*$.

FNM predictions at non-zero shear rate. – In the preceding sections a prediction for the stress tensor has been obtained using the FNM. The FNM was first derived in the context of perfectly rigid grains, and the effects of grain stiffness and system elasticity were incorporated by considering crossovers in characteristic length scales. The FNM prediction for the stress tensor is given by

$$\mathbf{\Sigma} \propto \begin{cases} \xi\dot{\gamma}^2, & \text{for } \xi \leqslant \Lambda; \\ c\dot{\gamma}, & \text{for } \xi \geqslant \Lambda \text{ and } l^* \geqslant \Lambda; \\ c^2/l^*, & \text{for } \xi \geqslant \Lambda \text{ and } l^* \leqslant \Lambda. \end{cases} \tag{3}$$

The variables ξ, c, and l^* depend on the viscoelastic grain properties and packing fraction, but not on $\dot{\gamma}$. A schematic of the length scales and flow regimes is shown in fig. 2.

The transitions between flow regimes can also be expressed in terms of the critical packing fractions $\phi_{\rm hs}$ and $\phi_{\rm qs}$, as defined in fig. 2. We focus here on the limit of stiff grains with $\Lambda \gg 1$. According to eq. (3), the transition from elastic-inertial scaling to quasi-static scaling occurs when $l^* = \Lambda$. Given that $l^* \propto (\phi - \phi_{\rm c})^{-1/2}$,

$$\phi_{\rm qs} - \phi_{\rm c} \propto (\dot{\gamma}/c)^2. \tag{4}$$

Similarly, the transition from Bagnold scaling to elastic-inertial scaling occurs when $\xi = \Lambda$. Since ξ diverges at $\phi_{\rm c}$, it scales as $\xi \propto (\phi_{\rm c} - \phi)^{-\psi}$ near the transition. This gives

$$\phi_{\rm c} - \phi_{\rm hs} \propto (\dot{\gamma}/c)^{1/\psi}. \tag{5}$$

Equations (4), (5) fully determine the crossovers in rheology and are used to construct the flow map in fig. 3.

For constant $\phi < \phi_{\rm c}$, corresponding to a horizontal slice through fig. 3, the system exhibits Bagnold scaling for small $\dot{\gamma}$ and elastic-inertial scaling for large $\dot{\gamma}$. This unexpected behavior where Bagnold's scaling, normally associated with "rapid" flows, actually occurs for small $\dot{\gamma}$ in constant volume shear flows has been observed previously [11]. For constant $\phi > \phi_{\rm c}$, the system exhibits quasi-static scaling for large $\dot{\gamma}$ and elastic-inertial scaling for small $\dot{\gamma}$. The emergence of quasi-static flow as the shear rate is reduced in dense materials is a feature that has been observed in experiments [14] and simulations [22]. Finally, for a flow with constant $\dot{\gamma} > 0$, the system passes through all three rheologies as the packing fraction is increased.

The preceding analysis only strictly holds for infinite system size L. For finite L we expect the rheology to depend on the size of the smallest length scale —$\xi(\phi)$, $\Lambda(\phi)$, or $l^*(\phi)$— compared to L. If $L > \Lambda(\phi_{\rm qs})$ there are no finite-size effects. If $L < \Lambda(\phi_{\rm qs})$ then finite-size effects become relevant at the packing fraction where $L = \xi(\phi)$ (for $L < \Lambda(\phi_{\rm hs})$) or $L = \Lambda(\phi)$ (for $L > \Lambda(\phi_{\rm hs})$), and persist until $L = l^*(\phi)$ in the quasi-static regime.

Of particular interest is $L < \Lambda(\phi_{\rm hs})$, in which case the elastic-inertial rheology is not observed. Instead, the system transitions from the Bagnold regime to the quasi-static regime with an intermediate phase that is system-size-dependent. Observables in the intermediate phase are determined by the finite-size scalings of the Bagnold and quasi-static regimes, and thus fluctuate between values characteristic of each regime. This behavior has been observed in simulations [23] and experiments [14]. Indeed, for experimental systems, $c \sim 100\,\mathrm{m/s}$ [24] so that for typical values of $\dot{\gamma} \sim 0.1\,\mathrm{s}^{-1}$, Λ is sufficiently large such that $L < \Lambda(\phi_{\rm hs})$. Therefore, we expect finite-size effects to be important in experimental systems. In order for the elastic-inertial regime to be observed in simulations [11], the stiffness of the grains must be very small, which reduces c and Λ. In this case, the stress tensor does not depend on L.

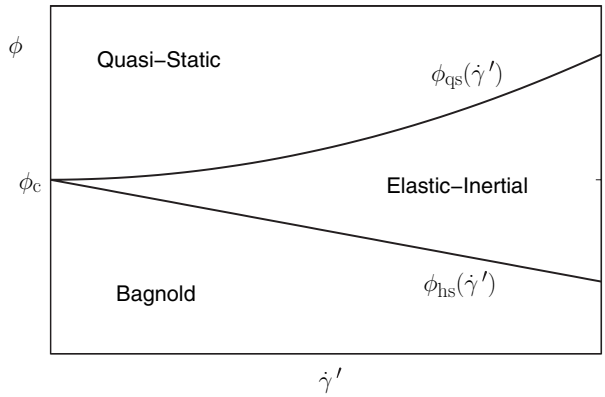

Fig. 3: The predicted flow map of sheared granular materials as a function of packing fraction ϕ and normalized shear rate $\dot{\gamma}' = \dot{\gamma}/c$. The scaling behavior of $\phi_{\rm qs}$ and $\phi_{\rm hs}$ are taken from eqs. (4), (5), using $\psi = 1$.

FNM predictions at zero shear rate. – In the limit of $\dot{\gamma} \to 0$ the FNM predicts that the yield pressure p_y and the yield shear stress s_y are each proportional to c^2/l^* for $\phi \geqslant \phi_{\rm c}$ (see footnote [1]). If a shear stress smaller than s_y is applied to the system it responds elastically with $s = G\gamma$, where G is the shear modulus and γ is the shear strain [5]. At a critical shear strain γ^* the system yields and it must be the case that $s_y = G\gamma^*$. Using this definition for γ^* we have that $s = s_y$ for $\gamma \geqslant \gamma^*$ and $s = G\gamma$ for $\gamma \leqslant \gamma^*$. The pressure only depends on the packing fraction and $p = p_y$ for all γ [5].

In the elastic regime where $s = G\gamma$, the speed of force propagation is set by the elastic shear wave speed $c \propto \sqrt{G}$. By enforcing continuity of c at $\gamma = \gamma^*$ we deduce that $c \propto \sqrt{G}$ for all $\phi > \phi_{\rm qs}$. Combined with $l^* \propto \delta z^{-1}$, we predict that

$$G \propto p/\delta z, \tag{6}$$

and

$$\gamma^* \propto \delta z. \tag{7}$$

[1] Note that in the limit of $\dot{\gamma} \to 0$ and $\phi = \phi_{\rm c}$, $c = 0$ and $\Lambda = c/\dot{\gamma}$ is indeterminate. Nevertheless eq. (3) correctly predicts that $\mathbf{\Sigma} = 0$, regardless of the value of Λ.

The first scaling relates the shear modulus to the pressure and excess coordination. It matches measurements from simulation for all dimensions and interaction potentials [5]. The second relation predicts the shear strain at which the system yields. Although this has not been measured, the FNM predicts that yielding is a purely geometric phenomena, unaffected by interaction potential, and gives a testable expression for its scaling behavior.

Conclusions. – We have taken a dynamic approach to the jamming transition using the FNM to predict the stress tensor in the flowing regime and then extrapolating our results to the jammed state. While this procedure was aimed at understanding athermal granular materials, a similar technique should apply in amorphous systems such as glasses that jam as the temperature is reduced. Since the isostatic length scale l^* exists for all jammed amorphous materials, the challenge is to identify relevant correlation lengths in the flowing regime and relate them to properties of interest. Jamming may then be universally understood as the crossover of correlations from flowing length scales to the isostatic length scale.

* * *

This work was supported by the William M. Keck Foundation, the MRSEC program of NSF under Award No. DMR00-80034, the James S. McDonnell Foundation, the David and Lucile Packard Foundation, and NSF Grant Nos. DMR-9813752, PHY99-07949 and DMR-0606092.

REFERENCES

[1] Liu A. J. and Nagel S. R., *Nature*, **396** (1998) 21; Liu A. J. and Nagel S. R. (Editors), *Jamming and Rheology: Constrained Dynamics on Microscopic Scales* (Taylor and Francis, London) 2001.

[2] Lois G., Lemaître A. and Carlson J. M., *Europhys. Lett.*, **76** (2006) 318.

[3] Silbert L. E., Liu A. J. and Nagel S. R., *Phys. Rev. Lett.*, **95** (2005) 098301; Ellenbroek W. G., Somfai E., van Hecke M. and van Saarloos W., *Phys. Rev. Lett.*, **97** (2006) 258001.

[4] Donati C., Glotzer S. C., Poole P. H., Kob W. and Plimpton S. J., *Phys. Rev. E*, **60** (1999) 3107; Berthier L. *et al.*, *Science*, **310** (2005) 1797; Pan A. C., Garrahan J. P. and Chandler D., *Phys. Rev. E*, **72** (2005) 041106.

[5] O'Hern C. S., Langer S. A., Liu A. J. and Nagel S. R., *Phys. Rev. Lett.*, **88** (2002) 075507; O'Hern C. S., Silbert L. E., Liu A. J. and Nagel S. R., *Phys. Rev. E*, **68** (2003) 011306.

[6] Zhang H. P. and Makse H. A., *Phys. Rev. E*, **72** (2005) 011301.

[7] Majmudar T. S., Sperl M., Luding S. and Behringer R. P., *Phys. Rev. Lett.*, **98** (2007) 058001.

[8] Lois G., Lemaître A. and Carlson J. M., *Phys. Rev. E*, **76** (2007) 021302.

[9] Wyart M., Nagel S. R. and Witten T. A., *Europhys. Lett.*, **72** (2005) 486; Wyart M., Silbert L. E., Nagel S. R. and Witten T. A., *Phys. Rev. E*, **72** (2005) 051306.

[10] Makse H. A., Gland N., Johnson D. L. and Schwartz L. M., *Phys. Rev. Lett.*, **83** (1999) 5070; Makse H. A., Gland N., Johnson D. L. and Schwartz L., *Phys. Rev. E*, **70** (2004) 061302; Head D. A., *Phys. Rev. E*, **72** (2005) 021303; Henkes S. and Chakraborty B., *Phys. Rev. Lett.*, **95** (2005) 198002; Schwarz J. M., Liu A. J. and Chayes L. Q., *Europhys. Lett.*, **73** (2006) 560; Toninelli C., Biroli G. and Fisher D. S., *Phys. Rev. Lett.*, **96** (2006) 035702.

[11] Campbell C. S., *J. Fluid Mech.*, **465** (2002) 261.

[12] Campbell C. S., *J. Fluid Mech.*, **539** (2005) 273.

[13] Babic M., Shen H. H. and Shen H. T., *J. Fluid Mech.*, **219** (1990) 81; Shen H. H. and Sankaran B., *Phys. Rev. E*, **70** (2004) 051308; Ketterhagen W. R., Curtis J. S. and Wassgren C. R., *Phys. Rev. E*, **71** (2005) 061307.

[14] Savage S. B. and Sayed M., *J. Fluid Mech.*, **142** (1984) 391; Babic M., Shen H. H. and Shen H. T., *J. Fluid Mech.*, **219** (1990) 81.

[15] Majmudar T. S. and Behringer R. P., *Nature*, **435** (2005) 1079.

[16] Geng J., Howell D., Longhi E., Behringer R. P., Reydellet G., Vanel L., Clement E. and Luding S., *Phys. Rev. Lett.*, **87** (2001) 035506; Geng J., Reydellet G., Clement E. and Behringer R. P., *Physica D*, **182** (2003) 274.

[17] Bouchaud J.-P., Claudin P., Levine D. and Otto M., *Eur. Phys. J. E*, **4** (2001) 451; Socolar J. E. S., Schaeffer D. G. and Claudin P., *Eur. Phys. J. E*, **7** (2002) 353; Otto M., Bouchaud J.-P., Claudin P. and Socolar J. E. S., *Phys. Rev. E*, **67** (2003) 031302.

[18] Lois G., Lemaître A. and Carlson J. M., *Phys. Rev. E*, **76** (2007) 021303.

[19] Campbell C. S., *Annu. Rev. Fluid Mech.*, **22** (1990) 57; Goldhirsch I., *Annu. Rev. Fluid Mech.*, **35** (2003) 267; Garzo V. and Dufty J. W., *Phys. Rev. E*, **59** (1999) 5895.

[20] Johnson P. C. and Jackson R., *J. Fluid Mech.*, **176** (1987) 67; Volfson D., Tsimring L. S. and Aranson I. S., *Phys. Rev. E*, **68** (2003) 021301.

[21] Moukarzel C. F., *Phys. Rev. Lett.*, **81** (1998) 1634; Roux J.-N., *Phys. Rev. E*, **61** (2000) 6802.

[22] Zhang D. Z., *J. Rheol.*, **44** (2000) 1019.

[23] Aharonov E. and Sparks D., *Phys. Rev. E*, **60** (1999) 6890.

[24] Liu C.-h. and Nagel S. R., *Phys. Rev. B*, **48** (1993) 15646.